



Ordovician cyanobacterial calcification: A marine fossil proxy for atmospheric CO₂

Lijing Liu^{a,*}, Liyuan Liang^b, Yasheng Wu^c, Xiqiang Zhou^c, Lianqi Jia^a, Robert Riding^d

^a State Key Laboratory of Continental Dynamics, Shaanxi Key Laboratory of Early Life and Environment, Department of Geology, Northwest University, Xi'an, 710069, China

^b Geoconsultants Corporation, Kevil, KY 42053, USA

^c Key Laboratory of Petroleum Resource Research, Institute of Geology and Geophysics, Chinese Academy of Sciences, Beijing, 100029, China

^d Department of Earth and Planetary Sciences, University of Tennessee, Knoxville, TN 37996-1526, USA

ARTICLE INFO

Article history:

Received 14 May 2019

Received in revised form 15 October 2019

Accepted 4 November 2019

Available online 14 November 2019

Editor: I. Halevy

Keywords:

calcification
cyanobacteria
CO₂
modelling
Ordovician
photosynthesis

ABSTRACT

Ordovician atmospheric CO₂ level was an important influence on climate and life. However, modelled estimates of Ordovician CO₂ differ widely and, in contrast to much of the subsequent Phanerozoic, they lack fossil proxy constraints. *In vivo* cyanobacterial sheath calcification, promoted by carbon dioxide concentrating mechanisms (CCMs), creates distinctive microfossils. These provide a direct ecophysiological link to ambient concentrations of CO₂ and, to a lesser extent, O₂. Cyanobacteria do not calcify at high CO₂ concentrations. Experiments show that CCMs can be induced in present-day cyanobacteria at CO₂ levels below ~10 times present atmospheric level (PAL) and that this promotes sheath calcification. We compiled a global database of cyanobacterial calcification in marine environments throughout the Ordovician (485–443 Myr ago) and compared it with modelled estimates of atmospheric CO₂ and O₂. These data show that many genera of marine calcified cyanobacteria reappeared from Cambrian Series 2 or first appeared globally during the late middle to late Upper Ordovician (late Darriwilian to late Katian) in carbonate platform facies, resulting in a previously unrecognized ten-fold increase in global diversity. Such a large increase in calcification suggests widespread induction of CCM expression in cyanobacteria, consistent with sustained decline in external CO₂ concentrations below ~10× PAL, together with increase in dissolved O₂ level, during the late Darriwilian, Sandbian and Katian stages, ~460–445 Myr ago. These cyanobacterial calcification fossil proxy data provide a first order constraint on modelled estimates of atmospheric CO₂ for the Ordovician. Estimated CO₂ outputs from COPSE and recent GEOCARB-based models are broadly consistent with this cyanobacterial calcification proxy for the Ordovician. In view of the long history of cyanobacteria, the calcified cyanobacterial proxy offers potential to assist interpretation of CO₂ deeper into geological time.

© 2019 Elsevier B.V. All rights reserved.

1. Introduction

Atmospheric CO₂ level is of wide interest as a driver of climate, both for present-day conditions and in the geological past (Berner, 1991). CO₂ level can be measured directly (e.g., from ice core) for the past 800 thousand years (Lüthi et al., 2008). Prior to that, over much longer timescales, atmospheric CO₂ can be estimated by geochemical modelling (e.g., Berner et al., 1983) or assessed indirectly from fossil and geochemical proxies (Royer, 2014). Proxies, particularly those that are fossil-based, have been widely used to

evaluate modelled estimates of atmospheric CO₂ and O₂ levels for the past ~420 Myr (Royer, 2014, fig. 4; Foster et al., 2017). Each proxy is likely to have its own advantages and limitations, such as time span of application, estimation error, and sensitivity to specific PCO₂ level (Royer, 2014; Witkowski et al., 2018). Earlier than this, during the late Cambrian and early Ordovician (~500–475 Myr ago (Ma)), modelled estimates (e.g., Berner, 2008; Royer, 2014, fig. 2a) suggest much higher CO₂ levels. So far as we are aware, fossil proxies have not yet been applied to modelled data for periods older than the Upper Ordovician (Royer, 2014, fig. 4; Foster et al., 2017; Witkowski et al., 2018). Here we use a proxy based on cyanobacterial photosynthesis to test modelled estimates of atmospheric CO₂ during the Ordovician.

* Corresponding author.

E-mail address: liulijing@nwu.edu.cn (L. Liu).

Estimates of atmospheric CO₂ based on geochemical modelling (and isotopic data, notably $\delta^{13}\text{C}$ and $\delta^{34}\text{S}$) for the early Palaeozoic suggest 'greenhouse' conditions during the Cambrian fuelled by elevated CO₂ (Bernier, 1990). More recent models indicate that decline below $\sim 10\times$ PAL CO₂ might have occurred during the Ordovician period (Bernier, 2008). During the same interval, marine oxygenation is estimated to have increased (Lee and Riding, 2018) in response to increased atmospheric O₂ (Edwards et al., 2017), and also due to decline in sea-surface temperature (Trotter et al., 2008; Mills et al., 2019, fig. 4b) which favours O₂ dissolution in water. Current perspectives suggest that the Ordovician (485–443 Ma) was a period of significant causally interconnected changes in the Earth's biotic, climatic, and environmental systems (Servais et al., 2010). These include exponential increase in marine animal genera described as the Great Ordovician Biodiversification Event ('GOBE', Webby et al., 2004). The relatively high temperatures promoted by elevated atmospheric CO₂ levels (Bernier, 1990) that may have slowed marine diversification during the middle and late Cambrian (Gill et al., 2011), ameliorated during the Ordovician. The establishment of moderate sea-surface temperatures in the middle Ordovician (Trotter et al., 2008) and increase in O₂ (Edwards et al., 2017; Lee and Riding, 2018) have been suggested as primary drivers of the GOBE. However, although cooling is likely to have promoted ocean overturn and marine oxygenation (Kah et al., 2016), it ultimately led to Hirnantian glaciation and end-Ordovician Mass Extinction, terminating the GOBE (Trotter et al., 2008; Vandenbroucke et al., 2010).

Thus, climate change in general and cooling in particular, linked to atmospheric CO₂ levels and marine oxygenation, are widely regarded as major controls on the significant changes in marine biodiversity reflected by both the GOBE and the end-Ordovician Mass Extinction. However, absolute levels of atmospheric CO₂ during the Ordovician remain uncertain, as shown by large differences among current modelled estimates (e.g., Bernier, 2008; Nardin et al., 2011; Arvidson et al., 2013; Royer et al., 2014; Edwards et al., 2017; Lenton et al., 2018). Here we apply a fossil proxy based on cyanobacterial photosynthetic CO₂ concentrating mechanism (CCM) induction, inferred from their *in vivo* sheath-calcification, for CO₂ decline below $\sim 10\times$ PAL. This is supported by present-day observations that, below this level of CO₂, bicarbonate uptake during cyanobacterial photosynthesis can induce calcification that produces distinctive microfossils (Riding, 2006). To this end, we comprehensively documented the global stratigraphic distribution of calcified cyanobacteria throughout the Ordovician (486–443 Ma). These data reveal large increase in cyanobacterial calcification ~ 460 –445 Ma, suggesting sustained decline in CO₂ below $\sim 10\times$ PAL during this interval. Some recent modelled estimates of atmospheric CO₂ are more consistent with this proxy-based interpretation than others.

2. Cyanobacterial calcification – a CO₂ proxy

Cyanobacterial photosynthesis involves carbon dioxide concentrating mechanisms (CCMs) that are postulated to be a response to lower levels of CO₂ and higher levels of O₂ than those encountered early in cyanobacterial evolutionary history (Badger and Price, 2003; Price et al., 2008; Raven et al., 2008; 2017). Badger and Price (2003) identified at least four modes of active inorganic carbon uptake among CCM components: two bicarbonate transporters and two CO₂ uptake systems associated with the operation of specialized NAD(P)H dehydrogenase complexes. The ability to utilize bicarbonate provides an additional, and in marine environments, abundant, source of inorganic carbon. However, in order to be made available to the primary carbon-fixing enzyme Rubisco (ribulose-1.5 biphosphate carboxylase-oxygenase), bicarbonate must first be converted to CO₂. This transformation, catalysed

by carbonic anhydrases, results in cytoplasmic dehydration of the bicarbonate and extracellular release of hydroxide (OH⁻) (Cannon et al., 2010). If ambient carbonate saturation is sufficiently elevated the resulting increase in pH can result in precipitation of CaCO₃ minerals adjacent to the cell (Thompson and Ferris, 1990). For example, *in vivo* sheath calcification in filamentous cyanobacteria results in distinctive aseptate tubular calcareous microfossils such as *Girvanella* (Riding, 2006). Estimates based on the CO₂ concentration difference between the external bulk phase and the active site of Rubisco suggest that 'a CCM is needed to give half the rate of CO₂-saturated photosynthesis in a cyanobacterium with the highest extant cyanobacterial Form IB Rubisco CO₂ affinity when the atmospheric CO₂ is <12 times present atmospheric level' (Raven et al., 2017). This is consistent with laboratory experiments indicating that CCM expression is induced when the external carbon dioxide concentration is equivalent to partial pressure of CO₂ less than $\sim 10\times$ PAL (Shibata et al., 2001; Badger et al., 2002, p. 169).

In essence, therefore, calcification in cyanobacteria can reflect atmospheric CO₂ due to their ability to actively import bicarbonate and intracellularly convert it to CO₂, thereby increasing pH in their surrounding protective sheaths and promoting calcification when pCO₂ is $< \sim 10\times$ PAL (Riding, 2006). It is important to note that CCMs are induced only when CO₂ is low, and that this can result in calcification only if ambient carbonate saturation is sufficiently elevated. Thus, based on current information, these processes of bicarbonate import and associated pH increase do not appear to occur if CO₂ levels are much above the $\sim 10\times$ PAL threshold. In addition, at higher CO₂, DIC levels corresponding to seawater pH ~ 8 , estimated for the Ordovician generally (e.g., Halevy and Bachan, 2017), would not be expected to buffer pH sufficiently to prevent sheath calcification. This has been shown by Arp et al. (2001) who reported that significant pH buffering does not occur until pCO₂ > 31.6 \times PAL. Such levels of CO₂ are well above the 10 \times PAL limit to cyanobacterial CCM induction. In summary, at 31.6 \times PAL, there would be an ample supply of CO₂ and cyanobacteria would have no need to deploy energy-expensive CCMs to obtain CO₂, and would instead rely on passive CO₂ diffusion. In these circumstances there would be no bicarbonate import or other physiological effects promoting calcification, and sheaths would remain uncalcified.

In addition to the availability of dissolved inorganic carbon, the functioning of Rubisco, and its ability to bind O₂ as well as CO₂ at the same site, has also conditioned the development of CCMs (Kaplan et al., 1980). When O₂, as well as CO₂, is bound, oxygenase activity competitively inhibits carbon fixation, resulting in loss of fixed carbon from the cell by photorespiration. Oxygenase activity increases with O₂ and slows carbon fixation. CCMs depress oxygenase activity by concentrating CO₂ at the site of Rubisco in the cell (e.g. Kaplan et al., 1980; Raven, 1997a; Kaplan and Reinhold, 1999).

Thus, decline in CO₂ and increase in oxygenation are both implicated in cyanobacterial CCM induction which, if ambient carbonate saturation state (Supplementary Discussion) is sufficiently elevated, can promote *in vivo* sheath calcification (Riding, 2006). Previously, the geological timing of cyanobacterial CCM induction has been inferred from modelled values of CO₂ (e.g., Raven, 1997a; Badger et al., 2002; Giordano et al., 2005). Here, in contrast, we use the geological occurrence of marine fossils produced by *in vivo* cyanobacterial sheath calcification to indicate atmospheric CO₂ level (Riding, 2006; 2009; Kah and Riding, 2007). We term this the 'cyanobacterial calcification proxy' and take it to broadly reflect CO₂ levels that were less than $\sim 10\times$ PAL (Badger et al., 2002, p. 169).

3. Methods

3.1. Global database of calcified cyanobacteria

Though calcified cyanobacteria are common fossils in the Ordovician, detailed assessment of their diversity and distribution have been hindered by difficulties in confidently recognizing their identities based on relatively simple and overlapping morphologies (Nitecki et al., 2004). Recent advances in systematic studies of Ordovician calcified cyanobacteria and their palaeoenvironmental and stratigraphic distributions in China (Liu et al., 2016a; 2016b; 2017; 2019), have greatly clarified identities, affinities and facies occurrences. Accordingly, we carried out a detailed literature search to compile comprehensive calcified cyanobacteria genus occurrence data for the entire Ordovician period by palaeogeographic region. These were used to create an integrated diversification curve accompanied by abundance data. We focused on genus-level to avoid subjective identification of these morphotypes at species-level. We followed the following protocol.

(i) To ensure accuracy we critically evaluated taxonomic identities from the literature. These were checked and, where appropriate, re-identified based on distinct morphologic features (e.g., filament arrangement, branching pattern, and size) (Liu et al., 2016a; 2019; Lee and Riding, 2016, and references therein). All re-identifications are noted in Table S1 and Supplementary Notes.

(ii) We only included taxa that could be confidently confirmed as calcified cyanobacteria based on the presence of micrite-impregnated sheaths of cyanobacterial appearance relative to extant filamentous cyanobacteria in freshwater karstic creeks and lakes (Arp et al., 2001; Riding, 2009; Lee and Riding, 2016; Liu et al., 2016a; 2019). We separately noted and identified occurrences of associated taxa of uncertain affinity (e.g., *Epiphyton*, *Garwoodia*, *Renalcis*, *Wetheredella*, and *Rothpletzella*) (Table S1) that have been compared at various times with calcified cyanobacteria, but which lack features diagnostic of extant calcified cyanobacteria, and/or possess features atypical of extant calcified cyanobacteria (Arp et al., 2001; Liu et al., 2016a; 2019).

(iii) We checked the age assignments of all of the fossils we recorded by reference to the original literature description, revising the age where appropriate (Table S1, Supplementary Notes). Revised ages and related references are included in Table S1. Reports of the ages of the genera are marked by dots in the column chart to at least stage-level.

(iv) To be aware of potential bias due to depositional environment, we investigated and noted, as accurately as possible, the sedimentary facies of each of the occurrences of calcified cyanobacteria included in our data compilation (Table S1). Based on similarities in the depositional records of facies types at different places and times (Flügel, 2004), we normalised these relative facies types as follows: reef (calcimicrobial reef, stromatolites, metazoan-algal dominated reef), open platform, bank, lagoon, tidal flats, mixed-platform, and drowned platform. We confirmed these carbonate facies in studies based on lithology, sedimentary structures, and community components, as has been done previously (Liu et al., 2017).

3.2. Dissolved oxygen estimates

We compared calcified cyanobacterial genus data with the following estimates of atmospheric CO₂: GEOCARBSULFvolc (Berner, 2008, fig 1b), GEOCLIM (Nardin et al., 2011, fig. 4), MAGic (Arvidson et al., 2013, fig 6A), GEOCARBSULF+GCM (Royer et al., 2014, fig 2A), updated GEOCARB (Edwards et al., 2017, fig. S1A), and COPSE (Lenton et al., 2018, fig 13A); and of O₂: GEOCARBSULF revised (Berner, 2009, fig. 2), MAGic (Arvidson et al., 2013, fig. 9A),

GEOCARBSULF+GCM (Royer et al., 2014, fig. 2B), updated GEOCARB (Edwards et al., 2017, fig S1B), COPSE (Lenton et al., 2018, fig. 13D), GEOCARBSULFOR (Krause et al., 2018, fig. 5), and photosynthetic fractionation effect model (Edwards et al., 2017, fig. S2). To convert modelled estimates of atmospheric O₂ (%) to dissolved oxygen (μM) in seawater we used a method similar to those described in Riding et al. (2019). Briefly, using the modelled atmospheric oxygen estimates, we applied Henry's law at 1 atmospheric pressure (i.e., sea surface), 35⁰/00 salinity and estimated sea surface temperature (Trotter et al., 2008) fitted by Pucéat et al. (2010). According to Henry's law, at constant temperature and pressure, the amount of O₂ gas that dissolves in water (C, μM) is directly proportional to the partial pressure of O₂ gas (pO₂) in equilibrium with water, i.e., $C = K_H \times pO_2$. Calculated K_H values were given previously (Riding et al., 2019) and are not repeated here.

4. Results

4.1. Secular distribution of Ordovician calcified cyanobacteria

We compiled and examined global data in the Ordovician fossil record (Table S1) by comprehensively reviewing and critically evaluating genus identification and age (see Methods and Supplementary Notes). Subsequently, we analysed the stratigraphic distribution and diversity of calcified cyanobacteria during this period.

During the Cambrian, calcified cyanobacteria appeared early in the period and reached an initial peak of diversity in Cambrian Series 2 (Riding, 2001). This includes nine genera (*Girvanella*, *Obruchevella*, *Razumovskia*, *Subtifloria*, *Bija*, *Hedstroemia*, *Batinevia*, *Botomaella*, and *Proaulopora*) (Riding and Voronova, 1985; Riding, 2001). By the late Cambrian (Furongian) these appear to have been reduced to a single genus (*Girvanella*) (Riding, 2001). Our data (Table S1 and supplementary notes) list a global total of 19 genera of cyanobacteria that can be classified as oscillatorialeans (Fig. 1) and nostocaleans (Fig. 2). They occur in Laurentia, North China, South China, Tarim, Siberia, Gondwana, and Kazakhstan (Fig. 3a). Their stratigraphic and facies occurrences are shown in Fig. 3b. The diversity of calcified cyanobacteria remained very low during the early Ordovician, with only *Girvanella* (Fig. 1a) and *Proaulopora* (Fig. 2a), although *Proaulopora* – not recorded since Cambrian Series 2 – is rare and only appears in open platform facies in the Floian in the Tarim Basin (Fig. 3b). This changed with marked diversity increase in the late Darriwilian when calcified cyanobacteria became widespread in lagoon, open platform, and reef facies (Fig. 3b). In addition to *Girvanella* and *Proaulopora*, further reappearances of Cambrian taxa were *Hedstroemia* (Fig. 2d) and *Subtifloria* (Fig. 1b) in the late Darriwilian, and *Bija* (Fig. 2e), *Razumovskia* (Figs. 1h, j), *Batinevia* (Fig. 1c), and *Obruchevella* (Fig. 1g) in the late Ordovician (Fig. 3b). At the same time, there also were significant first occurrences: *Bevoastria* (Fig. 1d), *Zonotrichites* (Fig. 2g), *Ortonella* (Fig. 2h), and *Phacelophyton* (Fig. 2b) in the late Darriwilian; *Cayeuxia* (Fig. 2f), *Acuasiphonoria* (Fig. 1i) and oscillatoriacean gen. indet 2 (Figs. 1l, m) in the Sandbian; and *Apophoretella* (Fig. 2i), *Gomphosphon* (Fig. 2c), *Xianella* (Figs. 1e, f), and oscillatoriacean gen. indet 1 (Fig. 1k) in many shallow-water facies in the Katian (Fig. 3b; Table S1). Several of these, such as *Girvanella*, *Subtifloria*, *Ortonella*, *Hedstroemia*, *Zonotrichites*, *Cayeuxia*, *Apophoretella* and *Bevoastria*, have been recorded in younger strata of Paleozoic and Mesozoic (Fig. 3b; Liu et al., 2016a). Overall, the integrated diversification data of calcified cyanobacteria show four stages: (I) very low values during the early Ordovician, and gradual increase toward the middle Ordovician, (II) sharp increase from the late Darriwilian (~460 Ma) that quadrupled the number of genera, and gradual increase to a peak in the early Katian (~453–450 Ma), (III) relatively steep and continuous decline from a peak to the end

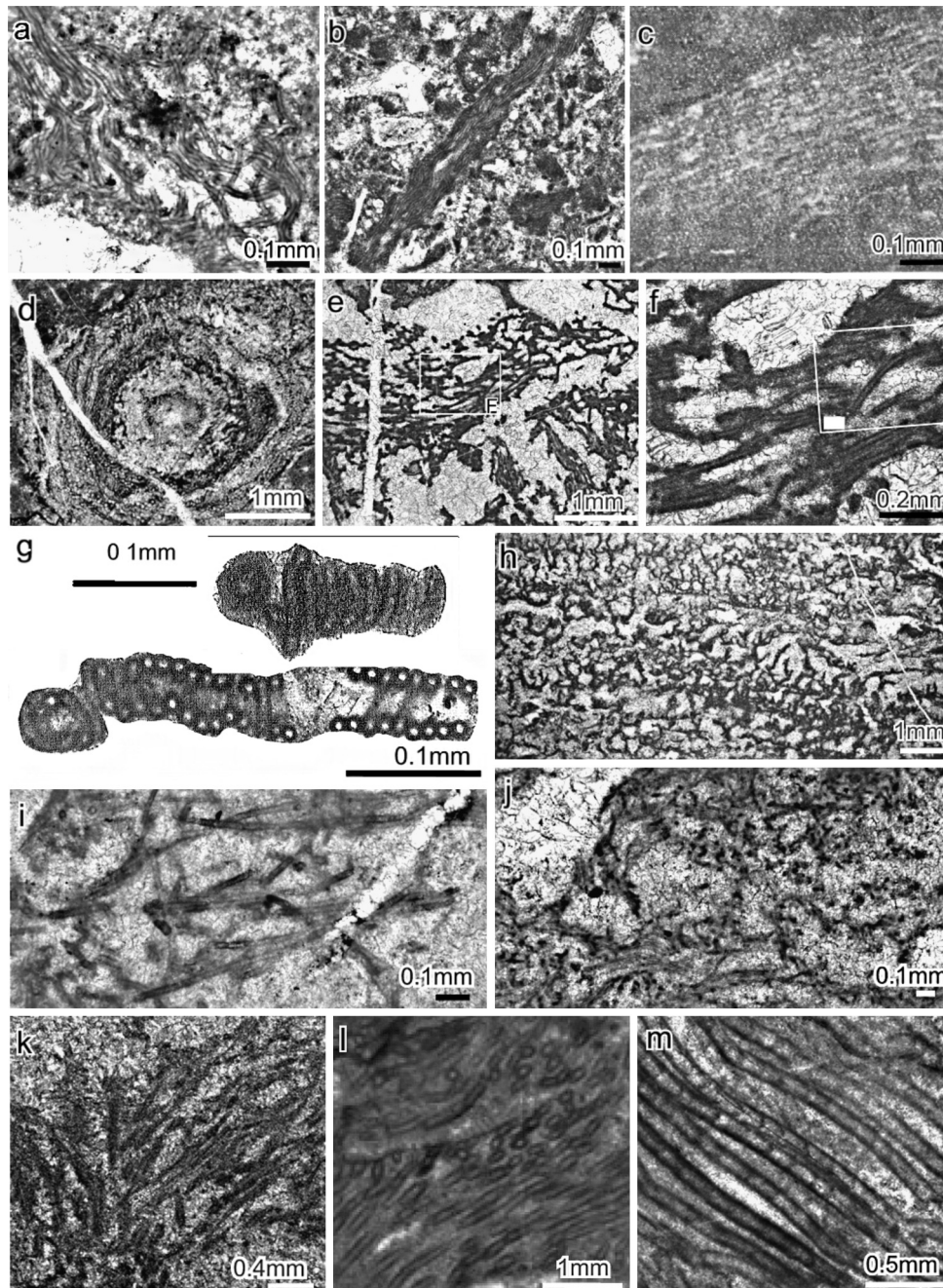


Fig. 1. Ordovician calcified oscillatoriacean cyanobacteria. a), *Girvanella*; b), *Subtifloria*; c), ?*Batinevia*; d), *Bevocastria*; e), f), *Xianella*; g), *Obruchevella*; h), j), *Razumovskia*; i), *Acuasiphonoria*; k), Oscillatoriaceae gen. indet. 1; l), m), Oscillatoriaceae gen. indet. 2 (c from Bian and Zhou, 1990; e, f from Lee and Riding, 2016; g from Mamet et al., 1992; k from Li et al., 2015; l, m from Lee et al., 2014; others from Liu et al., 2016a).

of the Katian (~445 Ma), with a loss of ~60% of genera, (IV) low diversity throughout the Hirnantian (~445–443 Ma) (Fig. 3b).

4.2. Ordovician cyanobacterial calcification episode

Although crustal block position, monographic variations, and local sedimentary facies likely influence the calcified cyanobacterial diversity data we obtained (Supplementary Discussion), the genus diversity trends based on the crustal blocks examined (especially in Tarim, South China, North China, and Laurentia) all broadly correspond in pattern of diversity increase from early to late Ordovician (Fig. 3b). Moreover, although the occurrences of calcified cyanobacteria are strongly related to sedimentary facies types, the integrated global diversification data largely exclude local facies

influences (Supplementary Discussion). Thus, our global diversification curve reflects the best currently available global pattern of cyanobacterial calcification for the Ordovician as a whole (Fig. 3b).

Riding (1992) recognized intervals of widespread abundance of calcified cyanobacteria in marine environments, termed them cyanobacterial calcification episodes (CCEs), and tentatively recognized the Cambrian-early Ordovician as an intense CCE, and the middle Ordovician-middle Devonian Stage as a reduced CCE. Arp et al. (2001), documenting the Phanerozoic record of sheath-calcified cyanobacterial fossils in more detail, confirmed Riding's (1992) broad recognition of CCEs. From the data of Arp et al. (2001, fig. 3d), the late Ordovician Katian peak of abundance of calcified cyanobacteria, and also Hirnantian decline can be recognized. Our data compilation reveals the scale of these changes more clearly.

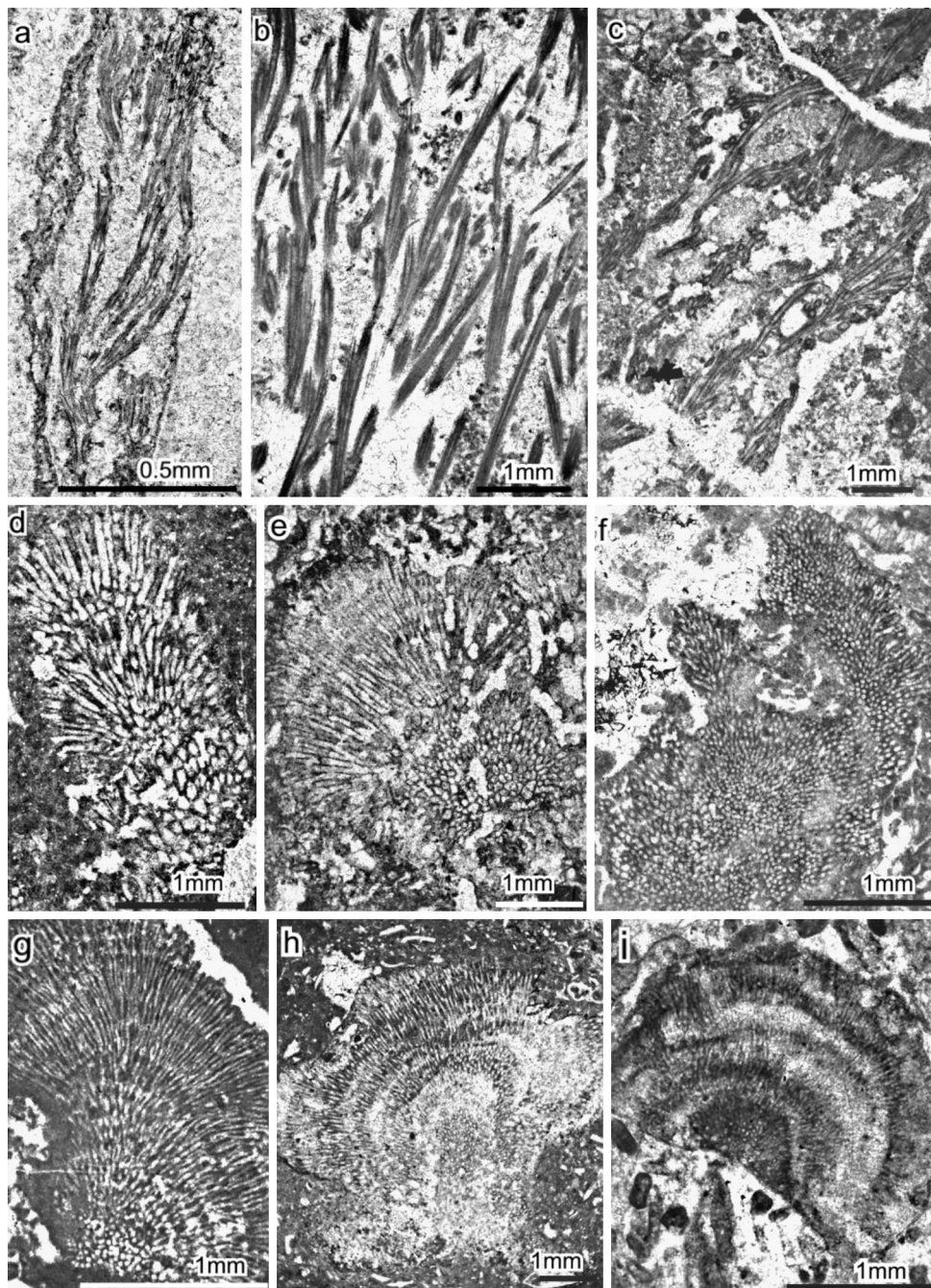


Fig. 2. Ordovician calcified nostocalean cyanobacteria. a), *Proaulopora*; b), *Phacelophyton*; c), *Gomphosiphon*; d), *Hedstroemia*; e), *Bija*; f), *Cayeuxia*; g), *Zonotrichites*; h), *Ortonella*; i), *Apophoretella*. (All from Liu et al., 2016a).

Following the early Ordovician- middle Darriwilian (stage I) reduced CCE, the late Darriwilian to late Katian (stages II-III) could be classed as an intense CCE *sensu* (Fig. 4a), when many genera reappeared since Cambrian Series 2 or firstly appeared during the interval of late Darriwilian to late Katian (Fig. 3b).

4.3. Proxy comparison with modelled CO_2 and O_2 estimates

In view of the elevated ambient carbonate saturation state throughout the Ordovician (Supplementary Discussion), the secular distribution of calcified cyanobacteria suggests the following changes in CO_2 and O_2 : (I) high CO_2 in the early, and most of the middle, Ordovician (and late Cambrian); (II)-(III) Subsequent decline in atmospheric CO_2 below $\sim 10\times$ PAL, and probably also

increase in dissolved O_2 level, during the late Darriwilian, Sandbian and Katian stages, ~ 460 – 445 Ma; (IV) either CO_2 increase or another factor, such as loss of habitat, that caused decline in cyanobacteria diversity during the late Katian and Hirnantian. Of these two possibilities, our preferred interpretation is loss of habitat due to sea-level fall during the well-documented Hirnantian glaciation (Supplementary Discussion). We have not studied Silurian calcified cyanobacteria, but they are reportedly abundant, although not especially diverse (Arp et al., 2001, Fig. 3D and supplementary data). Based on these limited data we would expect CO_2 to have remained near or below $\sim 10\times$ PAL during the Silurian to maintain cyanobacterial calcification.

We applied the cyanobacterial calcification proxy (Fig. 4a) to six modelled estimates of CO_2 (Fig. 4b): GEOCARBSULFvolc

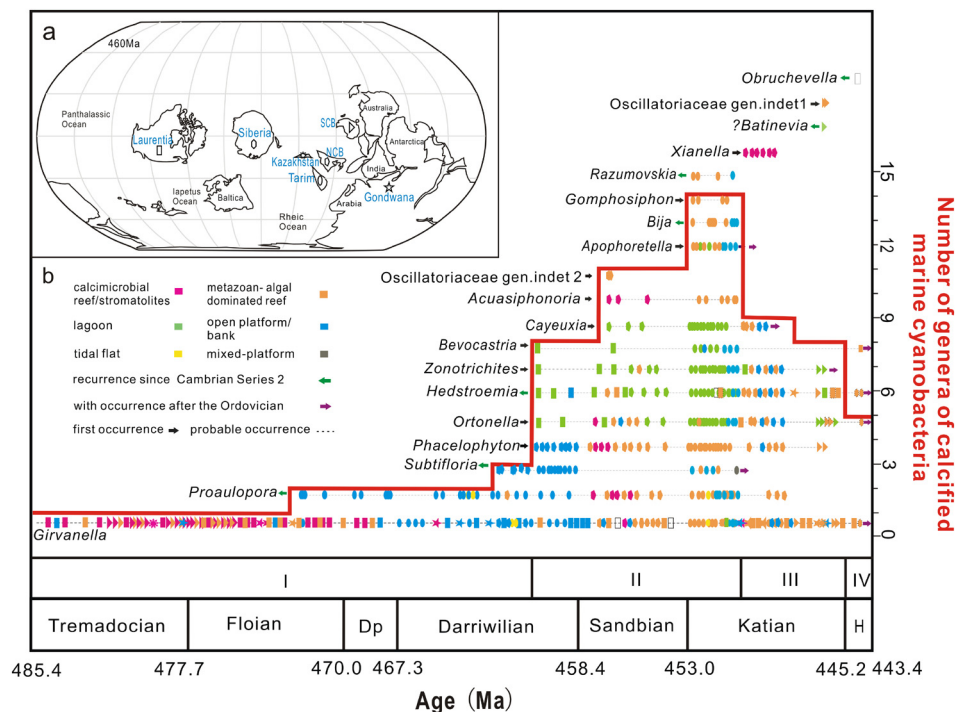


Fig. 3. a), Ordovician palaeogeographic positions of paleocontinents (based on Huang et al., 2018, fig. 4) with calcified cyanobacteria occurrences. Laurentia includes North America, Greenland, and slivers of crust in Norway and the British Isles; Gondwana includes South America, Africa, Antarctica, Australia and India (Servais et al., 2010). b), Secular global stratigraphic and sedimentary facies distribution of Ordovician calcified cyanobacteria, data from different regions illustrated by different shapes as marked in Fig. 3a (basing on Table S1).

(Berner, 2008), GEOCLIM (Nardin et al., 2011), MAGic (Arvidson et al., 2013), GEOCARBSULF+GCM (Royer et al., 2014), updated GEOCARB (Edwards et al., 2017), and COPSE (Lenton et al., 2018). In addition we compared the cyanobacterial calcification proxy to data from seven estimates of atmospheric O_2 (Fig. S1): GEOCARBSULF revised (Berner, 2009), MAGic (Arvidson et al., 2013), GEOCARBSULF+GCM (Royer et al., 2014), updated GEOCARB (Edwards et al., 2017), COPSE (Lenton et al., 2018), GEOCARBSULFOR (Krause et al., 2018), and photosynthetic fractionation effect model (Edwards et al., 2017), all of which we converted into dissolved O_2 values (Fig. 4d) (see Methods).

4.3.1. CO_2

The marked increase in calcified cyanobacterial diversity, observed during the late Darriwilian, Sandbian and Katian stages, ~460–445 Ma (Fig. 4a), suggests CCM induction in response to decline in CO_2 below $10\times$ PAL (Fig. 4b). The expectation, therefore, is for a broadly inverse relationship between the trends of CO_2 and calcified cyanobacterial abundance/diversity, with $10\times$ PAL CO_2 as the fulcrum of change. Two estimates (MAGic, GEOCLIM) maintain CO_2 above $10\times$ PAL throughout the Ordovician, and the remaining four estimates show CO_2 crossing this level from above to below (Fig. 4b). The crossing points are: 469.5 Ma (early Dapingian) for GEOCARBSULFvolc; 466.3 Ma (early Darriwilian) for GEOCARBSULF+GCM; 459 Ma (late Darriwilian) for updated GEOCARB; and 455.4 Ma (mid-Sandbian) for COPSE. Interestingly, as the publication date becomes younger, so does the estimated age of the crossing point. Furthermore, the two most recent publications, 'updated GEOCARB' and 'COPSE', which cross the $10\times$ PAL CO_2 threshold in the late Darriwilian (~460 Ma) and mid-Sandbian (~453 Ma) respectively, correspond most closely to the time of marked diversity increase in calcified cyanobacteria (Fig. 4a).

4.3.2. O_2

Increase in dissolved oxygen is thought to promote CCM induction (Kaplan and Reinhold, 1999; Giordano et al., 2005). Although we are not aware of an established threshold value, Badger et al. (2002, p. 169) suggested that near doubling of O_2 , together with CO_2 decrease, could trigger CCM induction. We evaluated atmospheric O_2 estimates from six geochemical models, and also from the photosynthetic fractionation effect model (Fig. S1). Among the estimates of atmospheric O_2 (Fig. S1), MAGic does not show any increase during the upper half of the Ordovician whereas 'GEOCARBSULF revised' shows slight increase for this interval, and three estimates show moderate increase in O_2 (GEOCARBSULF+GCM, COPSE, and GEOCARBSULFOR). The remaining two estimates that show steepest rise (discounting subsequent decline) are 'updated GEOCARB' (Edwards et al., 2017) and the photosynthetic fractionation effect model (Edwards et al., 2017). In general, these estimated trends show atmospheric O_2 either flat or rising during the Ordovician.

4.3.3. Dissolved O_2

Temperature decline during the Ordovician (e.g., Trotter et al., 2008; Fig. 4c) would allow more O_2 to dissolve in water, increasing marine oxygenation. All the models considered here (Fig. 4d), apart from MAGic, (i.e., GEOCARB-derived models and COPSE, particularly the more recently developed versions), indicate significant increase in oxygenation in the upper half of the Ordovician. For example, dissolved oxygen would be more than double its initial concentration based on the atmospheric estimates of O_2 from 'COPSE' and 'GEOCARBSULFOR' (~35 to 112 μM), and also from 'updated GEOCARB' and the photosynthetic fractionation effect model (105 to 248 μM). During this interval calcified cyanobacterial diversity also increased sharply, but then declined in the late Katian and Hirnantian.

Among the models considered here, COPSE (Lenton et al., 2018) and those derived from GEOCARB (Berner, 2008; Royer et al., 2014;

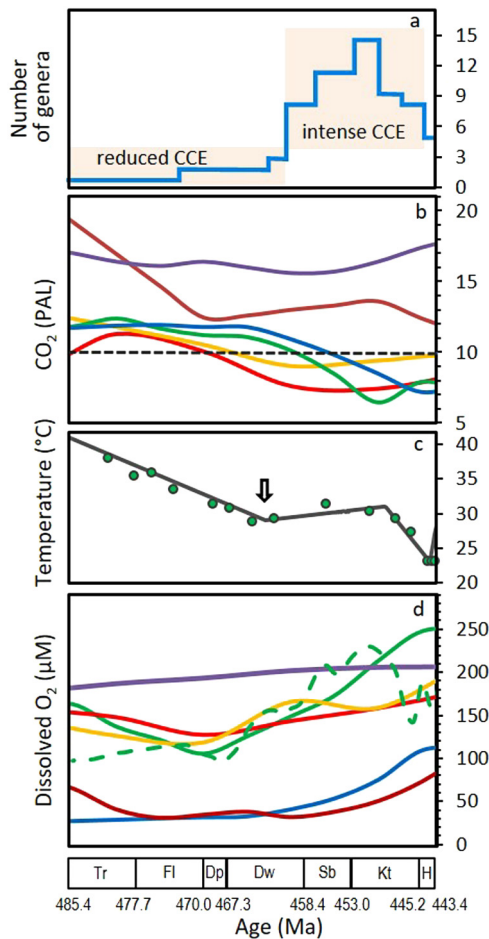


Fig. 4. Number of genera of calcified cyanobacteria compared with estimated atmospheric CO₂, dissolved oxygen and sea surface temperature during the Ordovician period. a), Number of genera of calcified cyanobacteria and cyanobacterial calcification episode (CCE, this study). b), Estimated atmospheric CO₂ (PAL): red, GEOCARBSULFvolc (Bernier, 2008); yellow, GEOCARBSULF+GCM (Royer et al., 2014); green, updated GEOCARB (Edwards et al., 2017); blue, COPSE (Lenton et al., 2018); purple, MAGIC (Arvidson et al., 2013); brown, GEOCLIM (Nardin et al., 2011). c), Estimated sea surface temperature: filled circles (Trotter et al., 2008); solid line, the same data fitted using equation from Pucéat (2010) (Edwards et al., 2017); the arrow showing the initiation of major biodiversity pulses of the GOBE (Trotter et al., 2008). d), Estimated dissolved oxygen (µM) based on modelled atmospheric O₂ and sea surface temperature (see Methods): red, GEOCARBSULF revised (Bernier, 2009); yellow, GEOCARBSULF+GCM (Royer et al., 2014); green, updated GEOCARB (Edwards et al., 2017); blue, COPSE (Lenton et al., 2018); purple, MAGIC (Arvidson et al., 2013); brown, GEOCARBSULFOR (Krause et al., 2018); dashed green line, photosynthetic fractionation effect model (Edwards et al., 2017). (For interpretation of the colors in the figure(s), the reader is referred to the web version of this article.)

Edwards et al., 2017), produce Ordovician CO₂ values broadly consistent with the cyanobacterial calcification proxy, whereas MAGIC (Arvidson et al., 2013) and GEOCLIM (Nardin et al., 2011) do not. With regard to dissolved O₂ levels, all models (Bernier, 2009; Royer et al., 2014; Edwards et al., 2017; Krause et al., 2018; Lenton et al., 2018) produce an upward trend during the second half of the Ordovician except MAGIC (Arvidson et al., 2013), which shows weak increase in dissolved O₂. At the same time, the more recent models (Krause et al., 2018; Lenton et al., 2018) yield O₂ levels generally lower (pO₂ < 12%, D.O. < 112 µM) than the earlier versions (pO₂ between 12 to 25%; D.O. between 104 to 248 µM). Overall, of the models considered here, the outputs from COPSE and recent GEOCARB-based models are most consistent with the cyanobacterial calcification proxy for the Ordovician. Of the modelled data assessed, most show values falling below 10× PAL during the Silurian: the exceptions are GEOCARBSULFvolc (Bernier, 2008) which

rises above 10× PAL during the Silurian, and GEOCLIM (Nardin et al., 2011) which declines to near 10× PAL at the Llandovery-Wenlock boundary, and then rises steeply. Edwards et al. (2017) updated GEOCARB also rises above 10× PAL in the early Llandovery but shows no younger data.

5. Discussion

5.1. Sedimentary facies and CCM induction

CCM induction allows cyanobacteria to overcome not only global reduction in CO₂ levels, but also local environmental CO₂ limitation at the scale of planktic blooms and microbial mat deposits (Raven, 1997b; Kaplan and Reinhold, 1999; Badger et al., 2002; p. 169; Badger and Price, 2003). This accounts for the persistence of calcified cyanobacteria during times when CO₂ is thought to have been globally elevated, e.g., late Cambrian (Riding, 2006, p. 309). Our data show calcified cyanobacteria in the early Ordovician were mostly limited to stromatolites (microbial mat carbonates) and metazoan reefs (Fig. 3b and Table S1), but subsequently became widely distributed in a range of open marine platform environments where CO₂ is not limited, such as calcareous algal and metazoan reef, open platform and lagoon (Fig. 3b and Table S1, Supplementary Discussion). This indicates that during the Darriwilian, Sandbian and Katian, CCM were widely induced in open marine conditions. This supports interpretation that the intense Darriwilian-Katian cyanobacterial calcification episode was a response to CCM induction linked global decline in atmospheric CO₂ to below 10× PAL.

5.2. The 10 × PAL CO₂ threshold

Once evolved, cyanobacterial CCMs are likely to have been retained and induced when necessary, depending on local as well as global conditions. The timing of the origin of cyanobacterial CCMs is poorly resolved (Burnap et al., 2015) but is inferred to reflect long-term changes in CO₂ and O₂ concentrations at the Earth's surface (Raven, 1991; 1997a; 1997b; Badger et al., 2002; Badger and Price, 2003). Based on the current modelled values of O₂ (Bernier, 2001) and CO₂ (Bernier and Kothavala, 2001, GEOCARB III), Badger et al. (2002, p. 169) suggested that 'large decline in CO₂ levels and an almost doubling of the O₂ concentration' would have applied pressure on photosynthetic organisms such as cyanobacteria to develop CCMs ~400 Ma. They inferred that this might have been the first time that CO₂ levels had ever been this low. However, using the cyanobacterial calcification proxy, Riding (2006) inferred CO₂ below 10× PAL ~800-700 Ma, and Kah and Riding (2007) extended this date back to at least ~1200 Ma. This is consistent with estimates from palaeosol mass balance and C-isotope reservoir modelling that suggest CO₂ of 7-10× PAL in the late Mesoproterozoic (Kah and Riding, 2007, fig. 3). It therefore appears that CO₂ levels declined during the Proterozoic, leading to the 'Snowball Earth' glaciations ~800-600 Ma, and to a cyanobacterial calcification episode that continued into the early Cambrian (Riding, 2006). CO₂ levels then rose significantly later in the Cambrian, as indicated by modelling (e.g., Bernier and Kothavala, 2001), before declining again in the Ordovician, resulting in increased cyanobacterial calcification ~460 Ma, as we suggest here (Fig. 4a).

The key assumption supporting these interpretations is the threshold below which CCM induction would be necessary in cyanobacteria, suggested by experiments to be ~10× PAL CO₂ (Shibata et al., 2001; Badger et al., 2002). Given its utility in assessing CO₂ levels at much earlier times than other current fossil proxies (Raven, 1997a; Raven et al., 2008), further work is needed to constrain the calcified cyanobacterial proxy, particularly recognizing that CCM induction is likely to differ not only according to

habitat, but also taxonomically (Raven et al., 2017). Similarly, the precise role of O₂, which is expected to increase selective pressure on cyanobacteria to counter photorespiration (Kaplan et al., 1980), in the evolution of CCMs also requires clarification (Giordano et al., 2005; Riding, 2006; Raven et al., 2008). It is known to supplement the inorganic carbon signal in at least one cyanobacterium (Woodger et al., 2005).

5.3. Comparative model evaluation

Long-term geochemical modelling of atmospheric CO₂ and O₂ endeavours to quantitatively deduce the production and cycling of these gases near the Earth's surface by applying the interactions of the physical, chemical and biological processes involved (Berner et al., 1983; Berner, 1999, 2006a,b; Mackenzie and Andersson, 2013; Royer et al., 2014; Lenton et al., 2018). From its inception, it has considered a wide variety of processes, such as solar radiation, seafloor spreading and sea-level change, chemical weathering and erosion of carbonate and siliciclastic rocks, sedimentary rock formation, volcanic degassing, effects of land plants, and burial and cycling of organic matter, etc. (Berner et al., 1983; Berner, 1991; 2003; Mackenzie and Andersson, 2013). This modelling work has largely concentrated on all or part of the Phanerozoic Eon (the past 541 Myr). GEOCARB (Berner, 1991), a long-established carbon cycle model initially focused on CO₂, was developed from the earlier BLAG model (Berner et al., 1983), and extended to O₂ by also considering the sulphur cycle (Berner and Canfield, 1989). There is now a family of GEOCARB-derived CO₂ and O₂ models (see Royer, 2014, pp. 252-254). The largest subset of the models we compared (Berner, 2008; Royer et al., 2014; Edwards et al., 2017; Krause et al., 2018) are GEOCARB-derived. Three others (GEOCLIM, Nardin et al., 2011; MAGic, Arvidson et al., 2013; COPSE, Lenton et al., 2018), are not.

Except for GEOCLIM, all the geochemical models considered here are non-dimensional box models, i.e., by placing C, S, etc. in reservoirs representing ocean, land, atmosphere, the model performs time-dependent mass balance among the reservoirs using material exchange (flux). This long-term biogeochemical cycling occurs through geological processes and geochemical reactions moving constituents from reservoir to reservoir. For example, GEOCARB involves the transfer of C- and S- containing gases to the atmosphere and oceans from deeply buried sedimentary rocks (including thermal decomposition of organic matter and pyrite) through diagenesis, metamorphism and volcanism. The C and S cycles are linked to oxygen since O₂ is removed when it oxidizes the reduced C and/or S-containing gases near the Earth's surface (Berner, 1999).

GEOCARB and its derivatives use a data-driven approach, in which the rock record and isotope data (e.g., $\delta^{13}\text{C}$, $\delta^{34}\text{S}$, $^{87}\text{Sr}/^{86}\text{Sr}$) are used to constrain the models' forcing functions and predict atmospheric CO₂ and O₂. In successive revisions, the model incorporated additional factors to constrain the modelled fluxes, with the aim of progressively improving earlier assumptions. For example, GEOCARB III (Berner and Kothavala, 2001), builds on GEOCARB II by incorporating results from the General Circulation Model (GCM), which couples CO₂ to global mean surface temperature and runoff, as well as solar radiation induced changes in temperature. Additionally, the model revision included, inter alia, (i) using Sr isotope data to constrain global physical erosion rate, (ii) the effects of large terrestrial plants on Ca-Mg silicate weathering, (iii) distinguishing volcanic weathering in subduction zones from the weathering of other silicates and seafloor basalt weathering, and (iv) updating the $\delta^{13}\text{C}$ values for limestones and organic matter.

Subsequent models also included tracking the transfer of carbon and sulphur between Earth surface (atmosphere, ocean, soil, living biomass) and rock reservoirs, both for reduced organic C and oxi-

dized carbonate C, and for reduced pyrite S and oxidized sulphate S (Berner, 2006a). Other modifications have included explicit expression of volcanic silicate weathering (Berner, 2006b), and incorporating improved estimates of land area, runoff, and continental temperature from the GCM (Royer et al., 2014). Thus, these models update process understanding through comparison with proxy data, thereby reducing the uncertainty of modelled results as new proxy data become available. Recently, Krause et al. (2018) attempted to predict Phanerozoic O₂ by replacing the sulphur cycle equations in GEOCARBSULF in line with forward modelling, utilizing an improved numerical scheme and the latest C isotope data. This use of new isotope data and other proxy data to improve modelling results is likely a key reason that these models yield CO₂ and O₂ values that agree more closely with the cyanobacterial calcification proxy.

In MAGic extensive inorganic reaction networks, coupling C to ten other elements, are used to predict CO₂, O₂ and seawater ionic compositions. Unlike the other geochemical models, it has limited treatment of biological processes, including organic matter. For example, P is considered in the model as a limiting nutrient for marine organic matter, but land plants and their burial fluxes are assumed to be small. The modelled results are compared with $\delta^{13}\text{C}$ values, fluid inclusion results and fossil records, but these data are not used to correct model parameters. GEOCLIM is a 3-dimensional (3D) model, using palaeogeographic information at a given geological time for five time slices in its modelling. It couples a 3D ocean-atmosphere model with a model of biogeochemical cycles of carbon and alkalinity. Although sophisticated, the omission of certain processes in these two models (e.g., the roles of biological processes and land plants on weathering are ignored in MAGic) could produce overall results that differ from our proxy data.

COPSE and MAGic, in comparison to the GEOCARB family, are forward models, relying less on proxy data as input parameters. However, these models adopt forcing functions from GEOCARB to predict CO₂, O₂ and seawater composition through time. In COPSE, for example, the predicted outputs of CO₂, O₂, SO₄, $\delta^{13}\text{C}$ data are compared with known isotope, fluid inclusion data and other proxies, to test process understanding. As necessary, the forcing functions are modified iteratively in these models. Again, these progressive modifications, as seen in the latest iteration of COPSE used here, bring the modelled data into closer agreement with the calcified cyanobacteria proxy. One recent development is the use of a more robust degassing input, derived from subduction zone length or flux constrained by $^{87}\text{Sr}/^{86}\text{Sr}$ values to revise COPSE and GEOCARBSULF (Mills et al., 2019). The new revisions improved temperature, as well as CO₂ predictions for 0-423 Ma, in which proxy data are available.

Generally, models predicting the long-term evolution of C cycle have improved with the incorporation of proxy data. Thus, iteration of models and new /or improved proxy data should enhance confidence in reconstructing past geochemical conditions of the Earth's surface.

6. Conclusions

Our CCM-based Ordovician cyanobacterial calcification proxy supports modelled estimates from GEOCARB-based (Berner, 2009; Royer et al., 2014; Edwards et al., 2017; Krause et al., 2018) and COPSE models (Lenton et al., 2018) that show decline in CO₂ below 10× PAL, together with increase in atmospheric O₂, between the late Darriwilian and Katian stages, ~460-445 Myr ago. It also supports the suggestion that CO₂ declined from 8× PAL in the Sandbian to ~5× PAL in the Hirnantian (Vandenbroucke et al., 2010). The substantial increase in marine cyanobacterial calcification during the interval of late Darriwilian to late Katian are consistent with long term reduction in sea-surface temperature

(Fig. 4c; Trotter et al., 2008) and increase in marine oxygenation (Fig. 4d; Edwards et al., 2017). Our findings strengthen the view that these factors also promoted late Darriwilian to Katian invertebrate diversification, major pulses of the GOBE (Fig. 4c; Trotter et al., 2008; Edwards et al., 2017; Lee and Riding, 2018). In addition, the subsequent reduction in diversity of calcified cyanobacteria observed during the late Katian and Hirnantian is consistent with continued decline in CO₂ and temperature that can be expected to loss of habitat during the Hirnantian glaciation, which is related to the end-Ordovician Mass Extinction – the most significant reduction in the Palaeozoic marine fauna prior to the late Permian. Our study also suggests that diversity rather than abundance data may provide more effective recognition criteria for cyanobacterial calcification episodes. This application of a fossil proxy to the elucidation of atmospheric CO₂ level qualifies modelled estimates and confirms fundamental environmental influence during a critical period in Earth's biotic history. In view of the long history of cyanobacteria, the calcified cyanobacterial proxy offers unusual potential to assist interpretation of CO₂ deep into geological time when other fossil proxies are lacking. It deserves further study, refinement and application.

Declaration of competing interest

The authors declare that they have no known competing financial interests or personal relationships that could have appeared to influence the work reported in this paper.

Acknowledgements

This work was supported by the National Natural Science Foundation of China (Grant No. 41502004, 41672025, 41720104002, 41890844, and 41972143) and Science Foundation of Shaanxi Province (Grant No. S2018-JC-YB-1007). We thank three anonymous reviewers for helpful comments and suggestions that helped us improve the final manuscript, and Itay Halevy for expert editorial guidance and encouragement.

Appendix A. Supplementary material

Supplementary material related to this article can be found online at <https://doi.org/10.1016/j.epsl.2019.115950>.

References

- Arp, G., Reimer, A., Reitner, J., 2001. Photosynthesis-induced biofilm calcification and calcium concentrations in Phanerozoic oceans. *Science* 292, 1701–1704.
- Arvidson, R.S., Mackenzie, F.T., Guidry, M.W., 2013. Geologic history of seawater: a MAGIC approach to carbon chemistry and ocean ventilation. *Chem. Geol.* 362, 287–304.
- Badger, M., Price, D., 2003. CO₂ concentrating mechanisms in cyanobacteria: molecular components, their diversity and evolution. *J. Exp. Bot.* 54, 609–622.
- Badger, M.R., Hanson, D., Price, G.D., 2002. Evolution and diversity of CO₂ concentrating mechanisms in cyanobacteria. *Funct. Plant Biol.* 29, 161–173.
- Berner, R.A., 1990. Atmospheric carbon dioxide levels over Phanerozoic time. *Science* 249, 1382–1386.
- Berner, R.A., 1991. A model for atmospheric CO₂ over Phanerozoic time. *Am. J. Sci.* 291, 339–376.
- Berner, R.A., 1999. Atmospheric oxygen over Phanerozoic time. *Proc. Natl. Acad. Sci. USA* 96, 10955–10957.
- Berner, R.A., 2003. The long-term carbon cycle, fossil fuels and atmospheric composition. *Nature* 426, 323–326.
- Berner, R.A., 2006a. GEOCARBSULF: a combined model for Phanerozoic atmospheric O₂ and CO₂. *Geochim. Cosmochim. Acta* 70, 5653–5664.
- Berner, R.A., 2006b. Inclusion of the weathering of volcanic rocks in the GEOCARBSULF model. *Am. J. Sci.* 306, 295–302.
- Berner, R.A., 2008. Addendum to 'Inclusion of the weathering of volcanic rocks in the GEOCARBSULF model' (R.A. Berner, 2006, v. 306, p. 295–302). *Am. J. Sci.* 308, 100–103.
- Berner, R.A., 2009. Phanerozoic atmospheric oxygen: new results using the GEOCARBSULF model. *Am. J. Sci.* 309, 603–606.
- Berner, R.A., Canfield, D., 1989. A new model for atmospheric oxygen over Phanerozoic time. *Am. J. Sci.* 289, 333–361.
- Berner, R.A., Kothavala, Z., 2001. GEOCARB III: a revised model of atmospheric CO₂ over Phanerozoic time. *Am. J. Sci.* 301, 182–204.
- Berner, R.A., Lasaga, A.C., Garrels, R.M., 1983. The carbonate-silicate geochemical cycle and its effect on atmospheric carbon dioxide over the past 100 million years. *Am. J. Sci.* 283, 641–683.
- Bian, L.Z., Zhou, X.P., 1990. Calcareous algae from the Sanqushan Formation (Upper Ordovician) at the border area between Zhejiang Province and Jiangxi Province. *J. Nanjing Univ. Geosci.* 2, 1–23 [in Chinese with English abstract].
- Burnap, R., Hagemann, M., Kaplan, A., 2015. Regulation of CO₂ concentrating mechanism in cyanobacteria. *Life* 5, 348–371.
- Cannon, G.C., Heinhorst, S., Kerfeld, C.A., 2010. Carboxysomal carbonic anhydrases: structure and role in microbial CO₂ fixation. *B. B. A.* 1804, 382–392.
- Edwards, C.T., Saltzman, M.R., Royer, D.L., Fike, D.A., 2017. Oxygenation as a driver of the Great Ordovician biodiversification event. *Nat. Geosci.* 10, 925–929.
- Flügel, E., 2004. *Microfacies of Carbonate Rocks: Analysis, Interpretation and Application*. Springer-Verlag, Berlin, Heidelberg, New York.
- Foster, G.L., Royer, D.L., Lunt, D.J., 2017. Future climate forcing potentially without precedent in the last 420 million years. *Nat. Commun.* 8, 14845.
- Gill, B.C., Lyons, T.W., Young, S.A., Kump, L.R., Knoll, A.H., Saltzman, M.R., 2011. Geochemical evidence for widespread euxinia in the later Cambrian ocean. *Nature* 469, 80–83.
- Giordano, M., Beardall, J., Raven, J.A., 2005. CO₂ concentrating mechanisms in algae: mechanisms, environmental modulation, and evolution. *Annu. Rev. Plant Biol.* 56, 99–131.
- Halevy, I., Bachan, A., 2017. The geologic history of seawater pH. *Science* 355, 1069–1071.
- Huang, B., Yan, Y., Piper, J.D.A., Zhang, D., Yi, Z., Yu, S., Zhou, T.H., 2018. Paleomagnetic constraints on the paleogeography of the East Asian blocks during Late Paleozoic and Early Mesozoic times. *Earth-Sci. Rev.* 186, 8–36.
- Kah, L.C., Riding, R., 2007. Mesoproterozoic carbon dioxide levels inferred from calcified cyanobacteria. *Geology* 35, 799–802.
- Kah, L.C., Thompson, C.K., Henderson, M.A., Zhan, R., 2016. Behavior of marine sulfur in the Ordovician. *Palaeogeogr. Palaeoclimatol. Palaeoecol.* 458, 133–153.
- Kaplan, A., Badger, M.R., Berry, J.A., 1980. Photosynthesis and the intracellular inorganic carbon-pool in the blue green algae *Anabaena variabilis*. Response to external CO₂ concentration. *Planta* 149, 219–226.
- Kaplan, A., Reinhold, L., 1999. The CO₂-concentrating mechanism of photosynthetic microorganisms. *Annu. Rev. Plant Physiol.* 50, 539–570.
- Krause, A.J., Mills, B.W.J., Zhang, S., Planavsky, N.J., Lenton, T.M., Poulton, S.W., 2018. Stepwise oxygenation of the Paleozoic atmosphere. *Nat. Commun.* 9, 4081.
- Lee, J.H., Riding, R., 2016. *Xianella*: a new mat-forming calcified cyanobacterium from the Middle-Late Ordovician of North China. *Palaeontol. Pap.* 2, 439–449.
- Lee, J.H., Riding, R., 2018. Marine oxygenation, lithistid sponges, and the early history of Paleozoic skeletal reefs. *Earth-Sci. Rev.* 181, 98–121.
- Lee, M., Sun, N., Choh, S.J., Lee, D.J., 2014. A new Middle Ordovician reef assemblage from north-central China and its palaeobiogeographical implications. *Sediment. Geol.* 310, 30–40.
- Lenton, T.M., Daines, S.J., Mills, B.J.W., 2018. Copse reloaded: an improved model of biogeochemical cycling over phanerozoic time. *Earth-Sci. Rev.* 178, 1–28.
- Li, Q., Li, Y., Kiessling, W., 2015. The first sphinctozoan-bearing reef from an Ordovician back arc basin. *Facies* 61, 17.
- Liu, L.J., Wu, Y.S., Bao, H.P., Jiang, H.X., Zheng, L.J., Chen, Y.L., 2019. Diversity and systematics of Middle-Late Ordovician calcified cyanobacteria and associated microfossils from Ordos Basin, North China. *J. Paleontol.* In press.
- Liu, L.J., Wu, Y.S., Jiang, H.X., Riding, R., 2016b. Calcified rivulariaceans from the Ordovician of the Tarim Basin, Northwest China, Phanerozoic lagoonal examples, and possible controlling factors. *Palaeogeogr. Palaeoclimatol. Palaeoecol.* 448, 371–381.
- Liu, L.J., Wu, Y.S., Jiang, H.X., Wu, N.Q., Jia, L.Q., 2017. Paleoenvironmental distribution of Ordovician calcimicrobial associations in the Tarim Basin, Northwest China. *Palaios* 32, 462–489.
- Liu, L.J., Wu, Y.S., Yang, H.J., Riding, R., 2016a. Ordovician calcified cyanobacteria and associated microfossils from the Tarim Basin, Northwest China: systematics and significance. *J. Syst. Paleontol.* 14, 183–210.
- Lüthi, D., Le Floch, M., Bereiter, B., Blunier, T., Barnola, J.M., Siegenthaler, U., Raynaud, D., Jouzel, J., Fischer, H., Kawamura, K., Stocker, T.F., 2008. High-resolution carbon dioxide concentration record 650,000–800,000 years before present. *Nature* 453, 379–382.
- Mackenzie, F.T., Andersson, A.J., 2013. The marine carbon system and ocean acidification during Phanerozoic time. *Geochem. Perspect.* 2, 1–227.
- Mamet, B., Roux, A., Lapointe, M., Gauthier, L., 1992. Algues Ordoviciennes et Siluriennes de l'île d'Anticosti (Québec, Canada). *Rev. Micropaléontol.* 35, 211–248.
- Mills, B.J.W., Krause, A.J., Scotese, C.R., Hill, D.J., Shields, G.A., Lenton, T.M., 2019. Modelling the long-term carbon cycle, atmospheric CO₂, and Earth surface temperature from late Neoproterozoic to present day. *Gondwana Res.* 67, 172–186.
- Nardin, E., Godderis, Y., Donnadieu, Y., Hir, G.L., Blakey, R.C., Puceat, E., Aretz, M., 2011. Modeling the early Paleozoic long-term climatic trend. *Geol. Soc. Am. Bull.* 123, 1181–1192.

- Nitecki, M.N., Webby, B.D., Spjeldnaes, N., Zhang, Y.Y., 2004. Receptaculitids and algae. In: Webby, B.D., Droser, M.L., Paris, F., Percival, I.G. (Eds.), *The Great Ordovician Biodiversification Event*. Columbia University Press, New York, pp. 336–347.
- Price, G.D., Badger, M.R., Woodger, F.J., Long, B.M., 2008. Advances in understanding the cyanobacterial CO₂-concentrating-mechanism (CCM): functional components, Ci transporters, diversity, genetic regulation and prospects for engineering into plants. *J. Exp. Bot.* 59, 1441–1461.
- Pucéat, E., Joachimski, M.M., Bouilloux, A., Monna, F., Bonin, A., Motreuil, S., Morinière, S., Hénard, J., Mourin, J., Dera, G., Quesne, D., 2010. Revised phosphate–water fractionation equation reassessing paleotemperatures derived from biogenic apatite. *Earth Planet. Sci. Lett.* 298, 135–142.
- Raven, J.A., 1991. Implications of inorganic carbon utilization: ecology, evolution, and geochemistry. *Can. J. Bot.* 69, 908–924.
- Raven, J.A., 1997a. Putting the C in phycology. *Eur. J. Phycol.* 32, 319–333.
- Raven, J.A., 1997b. The role of marine biota in the evolution of terrestrial biota: gases and genes. *Biogeochemistry* 39, 139–164.
- Raven, J.A., Beardall, J., Sánchez-Baracaldo, P., 2017. The possible evolution, and future, of CO₂-concentrating mechanisms. *J. Exp. Bot.* 68, 14.
- Raven, J.A., Cockell, C.S., De La Rocha, C.L., 2008. The evolution of inorganic carbon concentrating mechanisms in photosynthesis. *Philos. Trans. R. Soc. Lond. B* 363, 2641–2650.
- Riding, R., 1992. Temporal variation in calcification in marine cyanobacteria. *J. Geol. Soc. Lond.* 149, 979–989.
- Riding, R., 2001. Calcified algae and bacteria. In: Zhuravlev, A.Y., Riding, R. (Eds.), *Ecology of the Cambrian Radiation*. Columbia University Press, New York, pp. 445–473.
- Riding, R., 2006. Cyanobacterial calcification, carbon dioxide concentrating mechanisms, and Proterozoic–Cambrian changes in atmospheric composition. *Geobiology* 4, 299–316.
- Riding, R., 2009. An atmospheric stimulus for cyanobacterial-bioinduced calcification ca. 350 million years ago? *Palaios* 24, 685–696.
- Riding, R., Liang, L., Lee, J.-H., Virgone, A., 2019. Influence of dissolved oxygen on secular patterns of marine microbial carbonate abundance during the past 490 Myr. *Palaeogeogr. Palaeoclimatol. Palaeoecol.* 514, 135–143.
- Riding, R., Voronova, L., 1985. Morphological groups and series in Cambrian calcareous algae. In: Toomey, D.F., Nitecki, M.H. (Eds.), *Paleoalgology*. Springer-Verlag, Berlin, pp. 56–78.
- Royer, D.L., 2014. Atmospheric CO₂ and O₂ during the Phanerozoic: tools, patterns, and impacts. *Geochem. Treatise (Second Ed.)* 6, 251–267.
- Royer, D.L., Donnadieu, Y., Park, J., Kowalczyk, J., Goddérès, Y., 2014. Error analysis of CO₂ and O₂ estimates from the long-term geochemical model GEOCARBSULF. *Am. J. Sci.* 314, 1259–1283.
- Servais, T., Owen, A.W., Harper, D.A.T., Kröger, B., Munnecke, A., 2010. The Great Ordovician Biodiversification Event (GOBE): the palaeoecological dimension. *Palaeogeogr. Palaeoclimatol. Palaeoecol.* 294, 99–119.
- Shibata, M., Ohkawa, H., Kaneko, T., Fukuzawa, H., Tabata, S., Kaplan, A., Ogawa, T., 2001. Distinct constitutive and low-CO₂-induced CO₂ uptake systems in cyanobacteria: genes involved and their phylogenetic relationship with homologous genes in other organisms. *Proc. Natl. Acad. Sci. USA* 98, 11789–11794.
- Thompson, J.B., Ferris, F.G., 1990. Cyanobacterial precipitation of gypsum, calcite, and magnesite from natural alkaline lake water. *Geology* 18, 995–998.
- Trotter, J.A., Williams, I.S., Barnes, C.R., Lecuyer, C., Nicoll, R.S., 2008. Did cooling oceans trigger Ordovician biodiversification? Evidence from conodont thermometry. *Science* 321, 550–554.
- Vandenbroucke, T.R.A., Armstrong, H.A., Williams, M., Paris, F., Zalasiewicz, J.A., Sabbe, K., Nölvak, J., Challands, T.J., Verniers, J., Servais, T., 2010. Polar front shift and atmospheric CO₂ during the glacial maximum of the Early Paleozoic Icehouse. *Proc. Natl. Acad. Sci.* 107, 14983–14986.
- Webby, B.D., Paris, F., Droser, M.L., Percival, I.G., 2004. *The Great Ordovician Biodiversification Event*. Columbia University Press, New York, 497 pp.
- Witkowski, C.R., Weijers, J.W.H., Blais, B., Schouten, S., Sinninghe Damsté, J.S., 2018. Molecular fossils from phytoplankton reveal secular PCO₂ trend over the Phanerozoic. *Sci. Adv.* 4, 4556.
- Woodger, F.J., Badger, M.R., Price, G.D., 2005. Sensing of inorganic carbon limitation in *Synechococcus* PCC7942 is correlated with the size of the internal inorganic carbon pool and involves oxygen. *Plant Physiol.* 139, 1959–1969.